CHEMISTRY
A EUROPEAN JOURNAL

DOI: 10.1002/chem.200701942

Observation of Contraction and Expansion in a Bis(peptide)-Based Mechanical Molecular Actuator

Christian E. Schafmeister,*[a] Laura G. Belasco,[b] and Patrick H. Brown[c]

Abstract: A novel, bis(peptide) based molecular actuator (**1**) has been synthesized. It is demonstrated to undergo contraction and expansion controlled by the addition and removal of Cu^{2+}; this is demonstrated by the direct observation of a change in hydrodynamic properties by using sedimentation analysis and size exclusion chromatography. The molecule undergoes a large change in sedimentation coefficient, axial ratio, and size exclusion chromatography elution time when it binds copper. The demonstration of a controlled change in the mechanical properties of **1** make it a good starting point for the development of molecular devices that will harness changes in molecular shape and size to create molecular devices such as sensors or valves.

Keywords: bis(peptides) · host–guest systems · molecular devices · nanotechnology · sedimentation

Introduction

Mechanical molecular actuators are molecular devices that switch between two different conformational states under external control.[1–4] Molecular actuators have been developed that, in solution, change their color,[5] fluorescence properties,[6–10] chiroptical properties,[11] and electrical conductance[12] as they switch from one state to another. Many other groups[1,13–16] have created molecular devices that undergo a change in size and shape that is inferred indirectly from their property changes and from modeling; however, direct observations of shape changes of molecular devices in solution by measuring changes in hydrodynamic properties is lacking. Hydrodynamic measurements have been used for almost a century to demonstrate the existence of large conformational changes in proteins, such as myosin[17] and troponin C.[18] Because mechanical molecular actuators are developed to serve as components in rationally designed nanoscale devices, such as valves, hydrodynamic measurements can play a very useful role in optimizing their behavior.

In our laboratory, we have developed bis(amino acid) building blocks that allow us to create shape-persistent structures with designed function.[19] A goal of our laboratory is to use these building blocks to create molecular actuators that undergo a large change in shape and size, and to harness this conformational change to construct nanoscale valves and other active devices.[20,21] For example, nanoscale valves could be created that control the flow of proteins, peptides, and therapeutics for drug delivery by attaching the molecular actuators to the insides of nanoscale channels. When the actuators are switched through external control, they would contract against the wall of the channel to open the valve and expand into the center of the channel to close it. We wanted to see if we could create such a molecular actuator and demonstrate a change in shape and size in solution using sedimentation analysis and size exclusion chromatography.

Results and Discussion

Proteins that undergo large conformational changes have one state that is anisometric (length ⩾ width) and adopt a more symmetrical shape in their other state.[22] With this in mind, we designed and synthesized molecule **1** using solid-phase synthesis techniques. It consists of two molecular rods

[a] Prof. Dr. C. E. Schafmeister
Department of Chemistry, Temple University
1901 N. 13th Street, Philadelphia, PA 19122 (USA)
Fax: (+1) 215-204-1532
E-mail: meister@temple.edu

[b] L. G. Belasco
SAIC, 3465 Box Hill Corporate Center Drive
Abingdon, MD 21009 (USA)

[c] Dr. P. H. Brown
Protein Biophysics Resource
National Institute for Biomedical Imaging and Bioengineering
National Institutes of Health, Bethesda, MD 20892 (USA)

Supporting information for this article is available on the WWW under http://www.chemeurj.org/ or from the author.

approximately 24 Å[23] in length each containing four bis-(amino acid)[19] monomers connected by a flexible hinge consisting of an ornithine residue (Figure 1, Scheme 1). The two rods are structured domains that provide anisometry and shape persistence to the unbound form. The hinge will have a tendency to adopt an all *trans* conformation, which leads the unbound state to favor a more extended shape while being dynamic to allow the ends to come together to form a metal-binding site. The shape change of **1** is controlled by metal exchange. The two ends of **1** have two 5-carboxymethyl-8-hydroxyquinoline (Q) groups that together chelate a Cu^{2+} ion. 8-Hydroxyquinoline forms a very stable 2:1 complex with copper with a well-characterized square planar geometry.[24–26] We synthesized **1** as a linear oligomer on solid support and characterized it using high-perfor-

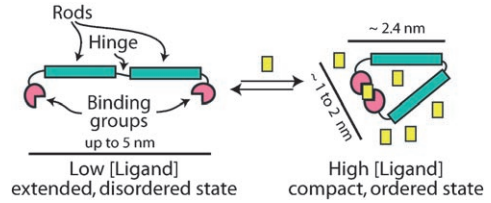

Figure 1. The operation of the hinged molecular actuator **1**.

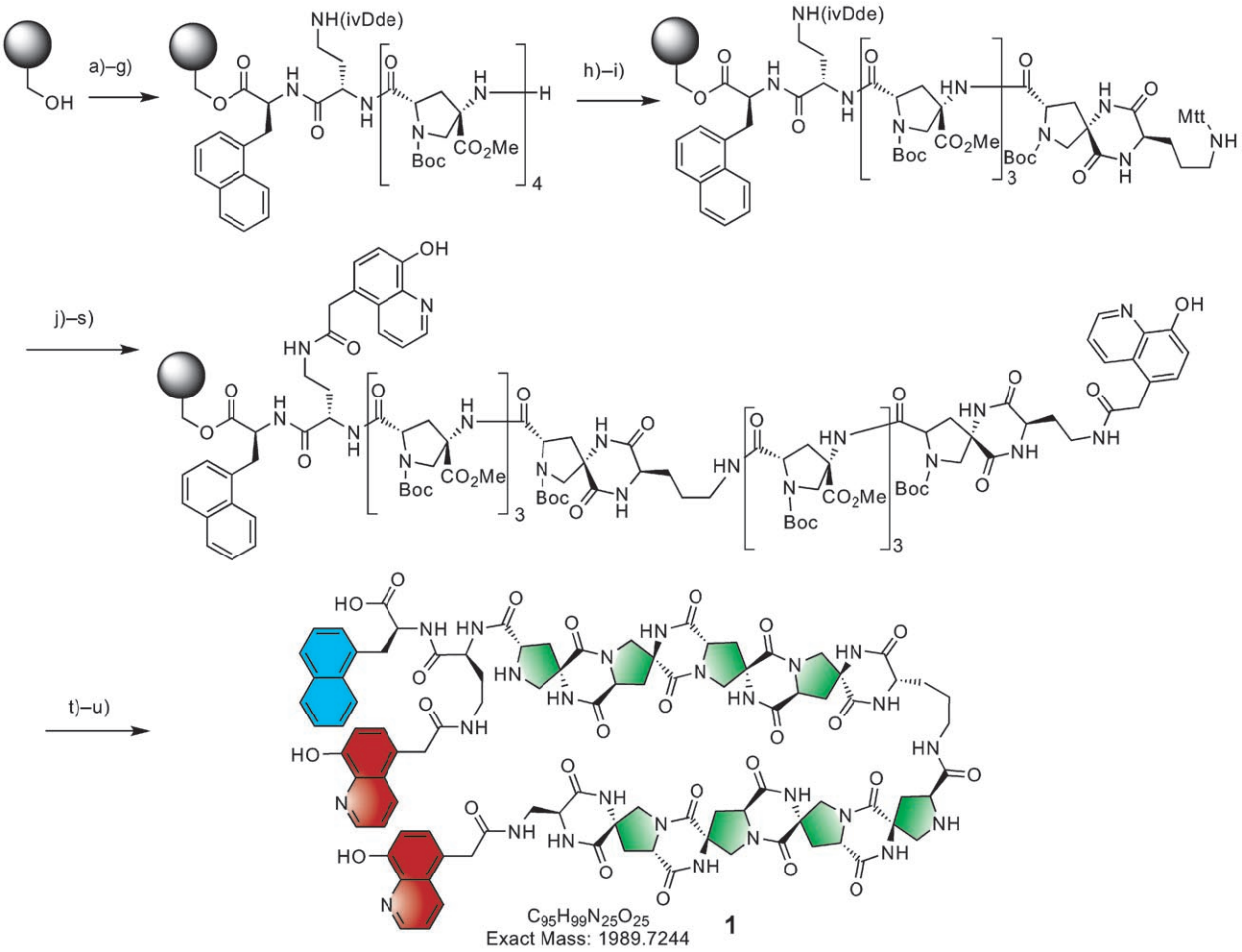

Scheme 1. Synthesis of **1** (see the Experimental Section for abbreviations). a) *N*-Fmoc-1-napthyl-L-alanine, MSNT, MeIm, CH_2Cl_2; for solid-phase synthesis b)–f) deprotection (piperidine (20%) in DMF, RT, 30 min), coupling (Fmoc-Xaa-OH (2 equiv; Xaa = *N*α-Fmoc-*N*γ-ivDde-L-diaminobutanioc acid (b), *N*α-Fmoc-*N*β-Boc pro4(2S4S) (c)–(f)), HATU (2 equiv), DIPEA (5 equiv), 0.2 M amino acid in 20% CH_2Cl_2/DMF, RT, 30 min, repeated to double couple each amino acid), and capping (50:12.5:1 DMF/Ac_2O/DIPEA (1 mL), RT, 20 min) steps were performed for each amino acid; g) deprotection (piperidine (20%) in DMF, RT, 30 min); h) coupling (*N*α-Fmoc-*N*δ-Mtt-L-ornithine (2 equiv), HATU (2 equiv), DIPEA (5 equiv), RT, 30 min, repeated once); i) piperidine (20%) in DMF, RT, 2 h; j) TFA (1%), triisopropylsilane (5%) in CH_2Cl_2 (1 mL), RT, 1 min, repeated 10 times; for solid phase synthesis k)–o) deprotection (piperidine (20%) in DMF, RT, 30 min), coupling (Fmoc-Xaa-OH (2 equiv; Xaa = *N*α-Fmoc-*N*β-Boc pro4(2S4S) (k)–(n), *N*α-Fmoc-*N*ε-Mtt-L-diaminopropionic acid (o)), HATU (2 equiv), DIPEA (5 equiv), RT, 30 min, repeated once), and capping (50:12.5:1 DMF/Ac_2O/DIPEA (1 mL), RT, 20 min) and deprotection (piperidine (20%) in DMF, RT, 30 min) steps were performed for each amino acid; p) piperidine/DMF (20%), RT, 1.5 h; q) TFA (1%), triisopropylsilane (5%) in CH_2Cl_2 (1 mL), RT, 1 min, repeated 10 times; r) hydrazine (2%) in DMF (1 mL), RT, 1 min, repeated 10 times; s) coupling (5-carboxymethyl-8-hydroxyquinoline (5 equiv), HATU (4.8 equiv), DIPEA (10 equiv), 0.2 M acid in 20% CH_2Cl_2/DMF, RT, 30 min) and aminolysis of phenolic esters (piperidine (20%) in DMF, RT, 5 min) steps were performed four times; t) TFA (80%), ethanedithiol (4%), thioanisol (8%), triflic acid (8%), 0 °C, 1 h; u) piperidine (20%) in DMF, RT, 36 h.

mance liquid chromatography, low-resolution mass spectrometry and high-resolution mass spectrometry.

Titration of **1** with Cu^{2+} shows spectral changes consistent with the formation of a [CuQ_2] complex (Figure 2).[27–29] Isosbestic points are observed at 250, 279, and 346 nm, which is consistent with a transition between two states. The absorption changes at 244 and 259 nm show an inflection point at a ratio of Cu^{2+} to **1** of 1.0 and little change beyond that when up to five equivalents of Cu^{2+} are added (Figure 3). Further addition of Cu^{2+} shows no other inflection points, implying no formation of 1:2 (**1**/Cu^{2+}) complexes. Addition of three equivalents of ethylenediaminetetraacetic acid (EDTA) to the metal-bound oligomer causes the spectrum to return to that of the metal-free species, which indicates that the switch is reversible (Figure 4). At concentrations higher than 100 μM, compound **1** is soluble, but aggregation occurs when copper is added.

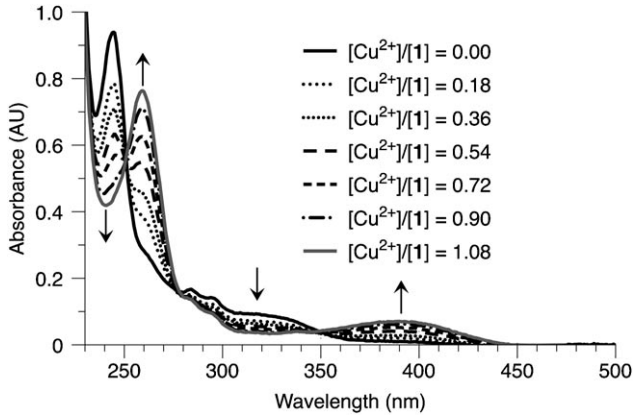

Figure 2. Spectrophotometric titration of a 17 μM solution of **1** (10 mM sodium phosphate, pH 7, T=25 °C) with a 150 μM solution of $CuCl_2$ showing the overlaid spectra. The arrows indicate the direction of change with increasing copper.

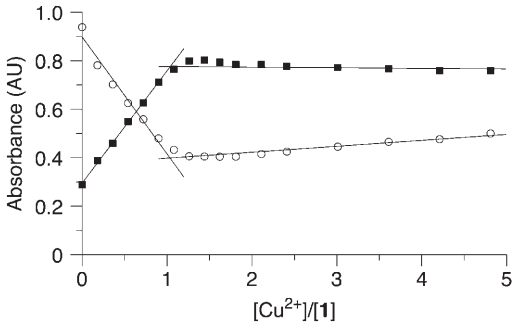

Figure 3. Spectrophotometric titration of **1** (17 μM solution of **1**, 10 mM sodium phosphate buffer, pH 7.0, T=25 °C, titrated with 150 μM $CuCl_2$) monitored at 244 nm (○) and 259 nm (■).

A Job analysis was performed to confirm the stoichiometry of copper binding to **1**.[30] The absorbance at 259 nm was plotted as a function of the mole fraction of **1** with respect to Cu^{2+} (Figure 5). The Job plot shows a maximum in absorbance at a mole fraction of 0.52, which is consistent with a binding stoichiometry of 1:1 (**1**/Cu^{2+}),

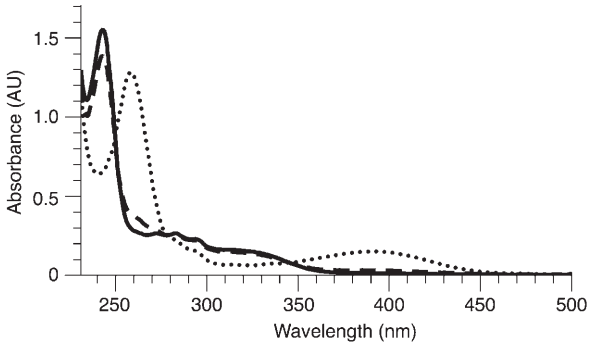

Figure 4. Three spectra that demonstrate the reversibility of copper binding to **1**. The spectrum of a 27 μM solution of **1** before the addition of copper (——), after addition of 1 equiv $CuCl_2$ (•••••), and after further addition of 3 equiv EDTA (-----).

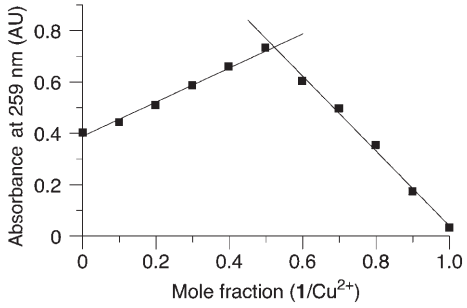

Figure 5. A Job plot of **1** combined with $CuCl_2$.

To determine the shape, size, and aggregation state of oligomer **1** in the metal-free and metal-bound states, we carried out sedimentation equilibrium and velocity experiments. A sample of **1** (7 μM **1**, 1.0 mM EDTA, 10 mM sodium phosphate buffer at pH 7.0) and a sample of **1**·Cu (5 μM **1**, 5 μM $CuCl_2$, 10 mM sodium phosphate buffer at pH 7.0) were centrifuged at 60000 rpm in a Beckman XL-I analytical ultracentrifuge for 20 h at room temperature. After this time, the samples had reached equilibrium, as indicated by a lack of change in the absorbance profile across the cell with increased time. We carried out sedimentation analysis using "Sedfit"[31] to determine the hydrodynamic parameters for **1** and **1**·Cu (see Table 1 and the Supporting Information).

Table 1. Hydrodynamic parameters for compounds **1** and **1**·Cu.

	ν_B [mL g^{-1}]	S[a]	Rs[b] [Å]	PAR a/b[c]	OAR a/b[d]
1	0.670	0.66	8.515 (8.51–8.52)	2.01	2.06
1·Cu	0.636	0.79	8.12 (8.08–8.16)	1.22	1.21

[a] Sedimentation coefficient given in Svedbergs (1x10^{-13} s) [b] Stokes radius, intervals represent one standard deviation [c] Prolate axial ratio, assuming 1.5% hydration. [d] Oblate axial ratio, assuming 1.5% hydration.

The analysis of the sedimentation equilibrium data indicates that both **1** and **1**·Cu are monomeric under these conditions. The sedimentation coefficient for **1**·Cu is 18% larger than that of **1**, which is consistent with the metal-free species being more extended and sedimenting slower due to increased hydrodynamic friction relative to the metal-bound species **1**·Cu. The predicted difference that would arise from an increase in mass due to a bound copper ion is 2.1%, assuming a proportional change in surface area and no change in overall shape. Therefore, a large conformational change upon binding the copper ion is necessary to account for the significant increase in the sedimentation coefficient.

The 18% relative change in sedimentation coefficient is large and comparable to relative changes seen in proteins that undergo large conformational changes when subjected to different conditions. Troponin C undergoes a large conformational change when it binds four Ca^{2+} ions and its sedimentation coefficient increases by 23%.[18] Smooth-muscle myosin undergoes a very large conformational change when it switches from its extended state to the more compact flexed state and its sedimentation coefficient increases by 50%.[17] Proteins such as citrate synthase and malate synthase that undergo significant but smaller conformational changes upon binding a ligand show small changes in sedimentation coefficient of 1.5 and −2% respectively.[32]

To further probe the differences in shape between the conformational states, shape modeling was performed by using the freeware program SEDNTERP.[33] The Stokes radius of **1** decreases by 4.7% upon binding copper, which is consistent with the molecule becoming more compact as it binds copper. The magnitude of the change is small because a sphere is a poor approximation of an anisometric molecule such as **1.** When we model the two states of the actuator as ellipsoids, a large change in axial ratio is necessary to account for the change in the sedimentation coefficient upon binding copper (Figure 6; the prolate axial ratio *a*/*b* for **1** is 2.03 and for **1**·Cu is 1.23).

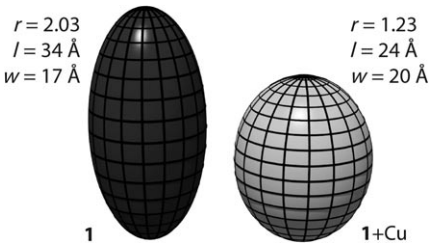

Figure 6. Cartoons of the two prolate ellipsoids *pe***1** (left, dark) and *pe***1**·Cu (right, light), which have the same hydrodynamic properties as **1** and **1**·Cu.

The contraction and expansion of **1** was further confirmed by using size exclusion chromatography; **1**·Cu elutes later than **1**, which is consistent with **1**·Cu being more compact and symmetric than **1** (Figure 7). Two resolved peaks were observed in the chromatogram of **1** with no added copper (solid chromatogram); analysis of the UV/Vis spectra indicated that the earlier peak at 36.6 min was metal-free **1** and the later peak at 38.9 min was very likely to be **1**·M (**1** bound to an unknown metal, probably copper from previous size exclusion runs). The observation of two resolved peaks indicates that the rate of metal exchange is slow relative to the chromatographic timescale, which is a desirable property for future valve applications.

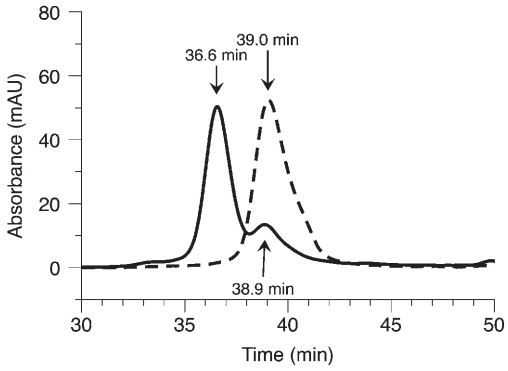

Figure 7. The size exclusion chromatograms of **1** with no added copper (——, monitored at 244 nm) and in the presence of one equivalent of $CuCl_2$ (----, monitored at 259 nm). The UV/Vis spectra of the peaks indicates that the peak at 36.6 min is metal-free **1**, the peak at 39.0 is **1**·Cu, and the peak at 38.9 min is very likely to be a contaminating metal-bound species **1**·M.

It is difficult to compare the performance of **1** with previously developed artificial molecular actuators because sedimentation analysis and size exclusion chromatography has not previously been used to characterize these types of molecules. Fluorescence resonant energy transfer (FRET) has been used to characterize molecular actuators,[3–7,10] but it suffers from a few drawbacks that compromise its value towards quantitatively determining distances and molecular dimensions. Quantitative analysis of FRET data is always frustrated by the uncertainty in the alignment of transition dipoles and the uncertainty in the amount of conformational flexibility that could change the time-average distance between the dye pair.[30] Sedimentation analysis and size exclusion chromatography do not suffer from these problems and they provide quantitative measures of the time-average dimensions of a molecule rather than just the distance between specific groups on a molecule. These techniques can provide valuable complementary data in the analysis of artificial molecular actuators and valuable data for the design of molecular devices that depend on a change in the physical dimensions of a molecular actuator, such as nanoscale valves.

Conclusion

We have constructed **1**, which is a water-soluble, hinged macromolecule that binds Cu^{2+}, and demonstrated directly using hydrodynamic measurements that it undergoes a large contraction and expansion under external control. It will serve as a starting point for future nanoscale mechanical

device applications that incorporate molecules which undergo large conformational changes.

Experimental Section

General: Solid-phase synthesis was performed in disposable polypropylene reaction columns connected to a three-way valve equipped with vacuum and argon for mixing. CH_2Cl_2 used in coupling reactions was distilled over calcium hydride. Dry grade dimethylformamide (DMF) used in coupling reactions was purchased from Aldrich. Diisopropylethylamine (DIPEA) was distilled under nitrogen sequentially from ninhydrin and potassium hydroxide and stored under molecular sieves. *O*-(7-Azabenzotriazon-1-yl)-*N*,*N*,*N*′,*N*′-tetramethyluronium hexafluorophosphate (HATU) was obtained from GenScript. 8-Hydroxyquinoline was obtained from Aldrich. All amino acids and resins were obtained from Novabiochem unless otherwise noted. The pro4(2S4S) monomer was synthesized by using literature procedures.[19] All solid-phase reactions were mixed by bubbling argon up through the reactor, which allowed mixing to occur and provided an inert atmosphere for the reaction.

HPLC–MS analysis was performed on a Hewlett–Packard 1050 HPLC/1100 electrospray MS instrument equipped with a Waters Xterra MS C18 column (3.5 μm packing, 4.6 mm × 100 mm) and a diode-array detector. High-resolution ESIMS was performed on a Waters LC/Q-TOF instrument. Preparative HPLC was performed on a Varian ProStar 500 HPLC system with an XTerra Prep MS C18 column (5 μm packing, 30 mm × 100 mm). UV/Vis experiments were performed on a Varian Cary 50 Bio spectrophotometer in 10 mm quartz cells. Gel filtration chromatography was performed on a Hewlett–Packard 1050 HPLC instrument equipped with a Superdex Peptide 10/300 GL column (13 μm packing, 10 mm × 300–310 mm). Analytical ultracentrifugation was performed on a Beckman Optima XL-I analytical ultracentrifuge. Data was analyzed using the programs SEDFIT,[34] SEDPHAT,[35] and SEDNTERP.[36]

The concentrations of all solutions of **1** in the absence of metal were determined by UV absorption at 25 °C by using the extinction coefficient ε_{244} ($2\times\varepsilon_{244}=56\,100\ \mathrm{L\,mol^{-1}\,cm^{-1}}$, determined at pH 7.0 from the slope of the calibration curve A_{244} versus concentration). The concentrations of all solutions of **1** in the presence of metal were determined by UV absorption at 25 °C by using the extinction coefficient ε_{259} ($2\times\varepsilon_{259}=49\,400\ \mathrm{L\,mol^{-1}\,cm^{-1}}$, determined at pH 7.0 from the slope of the calibration curve A_{259} versus concentration). All solutions for Job plots and titrations had concentrations in the micromolar range (10–50 μM) and were prepared in pH 7.0, 10 mM phosphate buffer. UV/Vis titrations were carried out by addition of standard metal solutions in water to the titration solution. The absorbance spectra were corrected for dilution and for the absorbance of the metal.

Solid-phase synthesis

General procedure A (HATU coupling): In a microcentrifuge tube, the amino acid (2 equiv) was dissolved in 20% CH_2Cl_2/DMF (0.2 M) with HATU (2 equiv). After mixing, DIPEA (5 equiv) was added and the solution was vortexed. The solution was left to sit for an activation time of 10 min, and it was then added to the resin and allowed to react under argon bubbling for 30 min followed by washing successively with 2 mL of CH_2Cl_2, CH_2Cl_2, *i*PrOH, CH_2Cl_2, and CH_2Cl_2 for 2 min each under argon bubbling. This coupling and washing step was repeated one additional time with the same amino acid.

General procedure B (capping): Unreacted amines were capped by the addition of 1 mL of a solution of 50:12.5:1 DMF/acetic anhydride/DIPEA with argon bubbling for 20 min followed by thorough washing successively with 2 mL of DMF, DMF, *i*PrOH, DMF, and DMF for 2 min each under argon bubbling.

General procedure C (9-fluoren-9-ylmethoxycarbonyl (Fmoc) deprotection): Deprotection of the Fmoc-protected amine was performed by the addition of 20% piperidine/DMF (1 mL) followed by argon bubbling for 30 min. The coupling yield was determined by measuring the absorbance of the piperidine/dibenzofulvene adduct ($\varepsilon_{301}=7800\ \mathrm{M^{-1}\,cm^{-1}}$) in this solution. The resin was then successively washed thoroughly with 2 mL of DMF, DMF, *i*PrOH, DMF, *i*PrOH, and DMF, DMF for 2 min each under argon bubbling.

Synthesis of 1: A 50 mg batch of hydroxymethyl polystyrene (100–200 mesh) resin (0.98 $\mathrm{mmol\,g^{-1}}$ substitution) was transferred to a solid-phase reaction vessel. The resin was swollen and the first amino acid, *N*-Fmoc-1-napthyl-L-alanine (42.9 mg, 98 μmol, Acros), was added to a solution of 1-(mesitylene-2-sulfonyl)-3-nitro-1*H*-1,2,4-triazole (MSNT), and 1-methylimidazole (MeIm) in CH_2Cl_2 (0.5 mL) and mixed by using a micropipettor in a 1.5 mL microcentrifuge tube (amino acid (5 equiv), MSNT (5 equiv), MeIm (3.75 equiv), 0.2 M amino acid in CH_2Cl_2). This solution was added to the resin and allowed to react under argon bubbling for 1 h followed by washing successively with 2 mL of CH_2Cl_2, CH_2Cl_2, *i*PrOH, CH_2Cl_2, and CH_2Cl_2 for 2 min each under argon bubbling. This coupling and washing step was repeated one additional time with the same amino acid. The sequence was then capped by using general procedure B and deprotected by using general procedure C.

*N*α-Fmoc-*N*γ-ivDde-L-diaminobutanoic acid (ivDde = 4,4-dimethyl-2,6-dioxocyclohex-1-ylidene; 21.4 mg, 39.2 μmol) was coupled to the resin by using general procedure A, and the sequence was capped by using general procedure B and deprotected by using general procedure C.

*N*α-Fmoc-*N*β-Boc pro4(2S4S) was coupled to the resin by using general procedure A. After capping by using general procedure B and deprotection by using general procedure C, these steps were repeated three more times for this residue, pro4(2S4S), to give a total of 4 pro4(2S4S) residues in a row.

*N*α-Fmoc-*N*δ-Mtt-L-ornithine (Mtt = methyltrityl; 23.9 mg, 39.2 μmol) was coupled to the resin by using general procedure A and capped by using general procedure B. The deprotection step (general procedure C), however, was extended from 30 min exposure to 20% piperidine to 2 h to allow for complete diketopiperazine formation. Capping by using general procedure B was then repeated, followed by a deprotection of the Mtt group by using 1% TFA and 5% TIS in CH_2Cl_2 (10 × 1 mL, 1 min each) under argon bubbling. The resin was then neutralized by using 5% DIPEA/CH_2Cl_2, 2 × 1 mL, 1 min each, under argon bubbling.

*N*α-Fmoc-*N*β-Boc pro4(2S4S) was coupled to the resin by using the general procedure A. After capping by using general procedure B and deprotection by using general procedure B, these steps were repeated three more times for this residue, pro4(2S4S), to give a total of 4 pro4(2S4S) residues in a row.

*N*α-Fmoc-*N*ε-Mtt-L-diaminopropionic acid (22.8 mg, 39.2 μmol) was coupled to the resin by using general procedure A and capped by using general procedure B. The deprotection step (general procedure C) was extended from 30 min exposure to 20% piperidine to 2 h to allow for complete diketopiperazine formation. The capping step was then repeated, followed by a deprotection of the Mtt group by using 1% TFA and 5% TIS in CH_2Cl_2, 10 × 1 mL, 1 min each, under argon bubbling. The resin was then neutralized by using 5% DIPEA/CH_2Cl_2, 2 × 1 mL, 1 min each, under argon bubbling. The *N*-ivDde protecting group on the second residue was then removed by using 2% hydrazine in DMF, 10 × 1 mL, 1 min each, under argon bubbling. The resin was then washed with 2 mL each of DMF, *i*PrOH, DMF, *i*PrOH, and DMF for 2 min each under argon bubbling.

5-Carboxymethyl-8-hydroxyquinoline (19.9 mg, 98 μmol) was coupled by using general procedure A, however, with acid (5 equiv), HATU (4.8 equiv), DIPEA (10 equiv), 0.2 M in 20% CH_2Cl_2/DMF. The resin was washed with 1 mL of 20% piperidine/DMF under argon bubbling to break up any 8-hydroxyquinoline phenyl ester polymeric chains that had formed on the resin. This coupling and washing step was repeated three additional times. The resin was then prepared for cleavage by washing with 2 mL each of DMF, *i*PrOH, DMF, *i*PrOH, CH_2Cl_2, MeOH, CH_2Cl_2, MeOH, and CH_2Cl_2 for 2 min each. The reactor was then put in a vacuum tube, and dried under reduced pressure overnight.

A small stirrer bar was added to the solid-phase reaction vessel, which was then capped and submerged in an ice bath. Ethanedithiol (12.5 μL) and thioanisole (25 μL) were added followed by trifluoroacetic acid (TFA; 250 μL) and triflic acid (25 μL). The cleavage solution was stirred

for 1 h at 0 °C and 1 h at room temperature and then filtered. The filtrate was then added dropwise into room temperature diethyl ether (15 mL). An additional 250 μL of TFA was added to the resin and filtered, then the TFA filtrate was added dropwise to the previous diethyl ether solution. The resulting precipitate was pelleted by centrifugation. The pellet was washed again with diethyl ether and dried to form a yellow residue through lyophilization. This residue was then dissolved in 20% piperidine/NMP (2 mL) and sealed in an HPLC vial with a diketopiperazine closure for 36 h at room temperature and monitored by LCMS. This solution was then added dropwise to diethyl ether, and the precipitate was pelleted by centrifugation. The product was purified by preparative HPLC (mobile phase, MeCN (0.05% formic acid)/H_2O (0.1% formic acid), 0% to 50% MeCN over 30 min; flow rate 25 mL min^{-1}). The desired fractions were concentrated by lyophilization to give a fluffy light yellow solid. The expected mass of **1** was confirmed by low-resolution HPLC–MS, illustrated in Figures S1 and S2 in the Supporting Information, as well as by high-resolution ESIMS (HR-ESIMS: m/z calcd for $C_{95}H_{101}N_{23}O_{25}$: 995.8700 [M+2H]/2, 664.2493 [M+3H]/3, 498.4389 [M+4]/4; found: 995.9069, 664.2669, 498.4535).

Spectrophotometric titration of 1: The nature of Cu^{2+} binding to **1** was studied by spectrophotometric titration of a 17 μM solution of **1** (10 mM sodium phosphate, pH 7, T=25 °C) with a 150 μM solution of $CuCl_2$ (Figure 2). Addition of copper causes the absorption band at 244 nm (due to the $\pi\rightarrow\pi^*$ transition of Q) to undergo a bathochromic shift to 259 nm, whereas the band at 315 nm decreases in intensity and a new metal-to-ligand charge-transfer band at 390 nm appears. Isosbestic points are observed at 250, 279 and 346 nm, which is consistent with a transformation between two unique species. A solution (100 μL) of **1** in 10 mM sodium phosphate buffer was placed in a quartz microcuvette. A UV/Vis spectrum was recorded at a rate of 600 nm min^{-1}, and the concentration of **1** was calculated from the absorbance at 244 nm. A standard solution of $CuCl_2$ in water (150 μM) was titrated into the solution of **1** a few microliters at a time with mixing by pumping the solution in and out with a 200 μL disposable pipette. Spectra were recorded after every addition of metal solution. All spectra were baseline subtracted by using a 10 mM sodium phosphate buffer blank and corrected for dilution.

The UV/Vis titration curves at 244 and 259 nm show an inflection point at a Cu^{2+}/**1** ratio of ≈1:1. Further addition of Cu^{2+} shows no other inflection points, which implies that there is no formation of 1:2 (**1**/Cu^{2+}) complexes (Figure 3).

Size exclusion chromatography: Size exclusion chromatography was performed on a Hewlett–Packard 1050 HPLC instrument equipped with a Superdex Peptide 10/300 GL column with a standard flow rate of 0.45 mL min^{-1} at 25 °C. The eluent used was 7 mM ammonium acetate buffer (pH 7.2) with 30% acetonitrile to reduce secondary interactions. While every effort was made to ensure that, with the choice of eluent, there would be no interactions with the column matrix, we discovered that the column has a slight ion exchange capability and that copper from earlier runs would be absorbed and released in later runs. We therefore washed the column with a 7 mM solution of EDTA (pH 7.0) containing 30% acetonitrile to remove residual metals as much as possible before the injection of the unbound actuator and then with a solution of 7 mM ammonium acetate buffer (pH 7.2) with 30% acetonitrile and 100 μM $CuCl_2$ to fill up the column's metal-chelating sites before injection of the bound actuator. This helped to ensure that the unbound actuator would not pick up any metal while in the column and the bound actuator would not lose any metal. However, metal contamination appeared to become more and more of a problem with continued use of the column. We believe that the small peak at 38.9 min in the copper-free sample (solid trace, Figure 7) is due to metal contamination because it became more prominent with repeated use of the column and because it has a UV/Vis spectrum with a λ_{max} at 259 nm, which is consistent with a metal-bound species. The metal-free versus metal-bound state was determined by measuring the absorption spectra of the peaks (see Figure S3 in the Supporting Information) and the exchange rate between the metal-bound species and the metal-free species was slower than the chromatographic timescale and so metal-bound and metal-free species were easily distinguished within individual runs by their different elution times and different absorbance spectra.

Analytical ultracentrifugation: An approach to a sedimentation equilibrium experiment was performed on both metal-free and copper-bound samples in 10 mM phosphate buffered saline (pH 7.0; see Figure S6 in the Supporting Information). A 0.5 mL sample of a solution of **1** (8 μM **1**, 1.0 mM EDTA, 10 mM phosphate buffer at pH 7.0) was dialyzed (2000 MWCO, 0.2–0.5 mL "Slide-a-lyzer" cassette, the cassette was prehydrated according to the manufacturer's instructions) against 100 mL of 1.0 mM EDTA, 10 mM phosphate buffer at pH 7.0 for 4 h. The final concentration of **1** in the sample was measured to be 7 μM, as determined by the UV/Vis absorbance at 244 nm. EDTA was added to the metal-free sample to scavenge metal introduced during dialysis. A 0.5 mL sample of a solution of **1**·Cu (16 μM 1, 20 μM $CuCl_2$, 10 mM phosphate buffer at pH 7.0) was dialyzed (2000 MWCO, 0.2–0.5 mL "Slide-a-lyzer" cassette, the cassette was prehydrated according to manufacturer's instructions) against 20 μM $CuCl_2$, 10 mM phosphate buffer at pH 7.0 for 4 h. The final concentration of **1** in the **1**·Cu sample was 5 μM, as determined by the UV/Vis absorbance at 259 nm. In the future we will use lower molecular weight cutoff dialysis membranes. The dialysates were used as blanks for analytical centrifugation. Sample (400 μL) and reference buffer (400 μL) were loaded into charcoal-filled double-sector epon centerpieces that had been thoroughly cleaned with an EDTA solution overnight. The loaded cells were then centrifuged at 60000 rpm, and absorbance measurements were recorded at radial increments of 0.001 cm every 300 s for 20 h at 20 °C in a Beckman XL-I analytical ultracentrifuge.

The compounds were determined to have been in sedimentation equilibrium (SE) once the root-mean-square (rms) difference between successive scans was below the level of noise in data acquisition (0.01OD). The SE scans were analyzed by using a discrete species model in SEDPHAT[35] to calculate a partial specific volume (ν_B) for each actuator with molecular weights fixed at the known values obtained from HRMS. Sedimentation coefficients for the metal-free (S=0.6601) and metal-bound (S=0.7891) actuator were determined by using the continuous distribution (c(s)) model in SedFit for scans covering the entire sedimentation process prior to reaching equilibrium. The values reported are the average of 1000 Monte Carlo simulations and the error intervals represent one standard deviation. The freeware program SEDNTERP[33] was used to calculate the frictional ratio, Stokes Radius (Rs), and maximum hydration of each actuator from the mass determined by HRMS, ν_B was calculated from SE, and the sedimentation coefficient was measured from the sedimentation velocity (SV) experiment. The errors in Rs reflect the variance in the sedimentation coefficient. The sedimentation equilibrium profiles (measured at 244 and 255 nm, respectively) from the metal-free and metal-bound samples are shown in Figure S8 in the Supporting Information. The absorbance spectra of the metal-free and metal-bound samples within the analytical centrifugation cells (after 20 h at 60,000 rpm) are shown in Figure S9 in the Supporting Information. Analysis of the sedimentation velocity/approach to equilibrium and sedimentation equilibrium data was performed using SedFit.[31]

We modeled the actuators as prolate ellipsoids using SEDNTERP and calculated the axial ratio for **1** and **1**·Cu as a function of hydration. Assuming 1.3% hydration, the prolate axial ratio for **1** is 2.03 and for **1**·Cu is 1.23. We modeled **1** and **1**·Cu as prolate and oblate ellipsoids using the following parameters: For **1**, M_r=1991 Da, s^*=0.66007 svedbergs, ν_B=0.6700 mL g^{-1}, ρ(density)=1.00523 g mL^{-1}, η(viscosity)=0.010189 poise; SEDNTERP calculated $R0=8.0867\times10^{-8}$ cm , $Rs=8.5157,\times10^{-8}$ cm. For 1·Cu, M_r=2052 Da, s^*=0.78913 svedbergs, ν_B=0.6355 mL g^{-1}, ρ(density)=1.00523 g mL^{-1}, η(viscosity)=0.010189 poise; SEDNTERP calculated $R0=8.0257\times10^{-8}$ cm, $Rs=8.1202\times10^{-8}$ cm. The degree of hydration (grams of bound water/grams of macromolecule) is an important parameter when carrying out shape modeling based on hydrodynamic parameters because predicted axial ratios decrease rapidly with increasing estimates of hydration (Figures S10 and S11 in the Supporting Information); this is one reason why it is best to compare hydrodynamic measurements in a relative mode rather than an absolute mode.[22] In the case of modeling **1** and **1**·Cu, the relative difference between predicted prolate axial ratios are large (>42%) and increase with increasing estimates of

hydration. At hydration values larger than approximately 2.5%, shape modeling of **1**·Cu gives non-physical predictions. We are assuming that hydration will be small because neither **1** nor **1**·Cu have pockets that can sequester water and that the level of hydration will not change when copper binds. We assumed a level of hydration of 1.5% for prolate ellipsoid and oblate ellipsoid shape modeling.

Acknowledgements

The authors acknowledge funding from the National Science Foundation under Grant Number 0348823. We acknowledge NIH Grant: 1S10RR017977-01 for high-resolution mass spectrometry. We thank Professor Catalina Achim for helpful suggestions.

[1] E. R. Kay, D. A. Leigh, F. Zerbetto, *Angew. Chem.* **2007**, *119*, 72–196; *Angew. Chem. Int. Ed.* **2007**, *46*, 72–191.
[2] Y. Liu, A. H. Flood, P. A. Bonvallet, S. A. Vignon, B. H. Northrop, H. R. Tseng, J. O. Jeppesen, T. J. Huang, B. Brough, M. Baller, S. Magonov, S. D. Solares, W. A. Goddard, C. M. Ho, J. F. Stoddart, *J. Am. Chem. Soc.* **2005**, *127*, 9745–9759.
[3] C.-F. Chow, S. Fujii, J.-M. Lehn, *Angew. Chem.* **2007**, *119*, 5095–5098; *Angew. Chem. Int. Ed.* **2007**, *46*, 5007–5010.
[4] Elena Kolomiets, V. Berl, J.-M. Lehn *Chem. Eur. J.* **2007**, *13*, 5466–5479.
[5] R. A. Bissell, E. Cordova, A. E. Kaifer, J. F. Stoddart, *Nature* **1994**, *369*, 133–137.
[6] T. E. Glass, *J. Am. Chem. Soc.* **2000**, *122*, 4522–4523.
[7] C. Monahan, J. T. Bien, B. D. Smith, *Chem. Commun.* **1998**, 431–432.
[8] H. Yuasa, N. Miyagawa, T. Izumi, M. Nakatani, M. Izumi, H. Hashimoto, *Org. Lett.* **2004**, *6*, 1489–1492.
[9] R. Krauss, H. Weinig, M. Seydack, J. Bendig, U. Koert, *Angew. Chem.* **2000**, *112*, 1905–1908; *Angew. Chem. Int. Ed.* **2000**, *39*, 1835–1837.
[10] V. A. Azov, A. Schlegel, F. Diederich, *Angew. Chem.* **2005**, *117*, 4711–4715; *Angew. Chem. Int. Ed.* **2005**, *44*, 4635–4638.
[11] G. Bottari, D. A. Leigh, E. M. Perez, *J. Am. Chem. Soc.* **2003**, *125*, 13360–13361.
[12] C. P. Collier, E. W. Wong, M. Belohradský, F. M. Raymo, J. F. Stoddart, P. J. Kuekes, R. S. Williams, J. R. Heath, *Science* **1999**, *285*, 391–394.
[13] M. C. Jimeñez, C. Dietrich-Buchecker, J. P. Sauvage, *Angew. Chem.* **2000**, *112*, 3422–3425; *Angew. Chem. Int. Ed.* **2000**, *39*, 3284–3287.
[14] N. Koumura, R. W. J. Zijlstra, R. A. van Delden, N. Harada, B. L. Feringa, *Nature* **1999**, *401*, 152–155.
[15] V. Serreli, C. F. Lee, E. R. Kay, D. A. Leigh, *Nature* **2007**, *445*, 523–527.
[16] J. D. Badjic, V. Balzani, A. Credi, S. Silvi, J. F. Stoddart, *Science* **2004**, *303*, 1845–1849.
[17] K. M. Trybus, T. W. Huiatt, S. Lowey, *Proc. Natl. Acad. Sci. USA* **1982**, *79*, 6151–6155.
[18] I. C. Kuo, C. J. Coffee, *J. Biol. Chem.* **1976**, *251*, 6315–6319.
[19] C. G. Levins, C. E. Schafmeister, *J. Am. Chem. Soc.* **2003**, *125*, 4702–4703.
[20] T. D. Nguyen, H.-R. Tseng, P. C. Celestre, A. H. Flood, Y. Liu, J. F. Stoddart, J. I. Zink, *Proc. Natl. Acad. Sci. USA* **2005**, *102*, 10029–10034.
[21] N. Liu, B. R. Dunphy, P. Atanassov, S. D. Bunge, Z. H. U. Chen, G. P. Lopez, T. J. Boyle, C. J. Brinker, *Nano Lett.* **2004**, *4*, 551–554.
[22] N. Errington, A. J. Rowe, *Eur. Biophys. J.* **2003**, *32*, 511–517.
[23] S. Pornsuwan, G. Bird, C. E. Schafmeister, S. Saxena, *J. Am. Chem. Soc.* **2006**, *128*, 3876–3877.
[24] R. C. Hoy, R. H. Morriss, *Acta Cryst.* **1967**, *22*, 476–482.
[25] J. A. Bevan, D. P. Graddon, J. F. McConnell, *Nature* **1963**, *199*, 373–373.
[26] A. Albert, *Biochem. J.* **1953**, *54*, 646–654.
[27] J. P. Phillips, W. H. Huber, J. W. Chung, L. L. Merritt, *J. Am. Chem. Soc.* **1951**, *73*, 630–632.
[28] K. Sone, *J. Am. Chem. Soc.* **1953**, *75*, 5207–5211.
[29] R. M. Watson, Y. A. Skorik, G. K. Patra, C. Achim, *J. Am. Chem. Soc.* **2005**, *127*, 14628–14639.
[30] C. Y. Huang, *Methods Enzymol.* **1982**, *87*, 509–525.
[31] P. Schuck, *Biophys. J.* **2000**, *78*, 1606–1619.
[32] H. Durchschlag, P. Zipper, G. Purr, R. Jaenicke, *Colloid Polym. Sci.* **1996**, *274*, 117–137.
[33] T. M. Laue, B. D. Shah, T. M. Ridgeway, S. L. Pelletier in *Analytical Ultracentrifugation in Biochemistry and Polymer Science* (Eds.: S. E. Harding, A. J. Rowe, J. C. Horton), Royal Society of Chemistry, Cambridge, **1992**, pp. 90–125.
[34] P. Schuck, http://www.analyticalultracentrifugation.com/default.htm
[35] P. Schuck, *Anal. Biochem.* **2003**, *320*, 104–124.
[36] J. S. Philo, http://www.jphilo.mailway.com/download.htm#SEDNTERP

Received: December 8, 2007
Published online: June 2, 2008

